ORIGINAL RESEARCH

Identification and Characterization of Genes Associated with Intestinal Ischemia-Reperfusion Injury and Oxidative Stress: A Bioinformatics and Experimental Approach Integrating High-Throughput Sequencing, Machine Learning, and Validation

Yongguo Xie[1,]*, Mingpu Yang[2,]*, Juanjuan Huang[3], Zongbin Jiang[4]

[1]Department of Anesthesiology, The Second Affiliated Hospital of Guangxi Medical University, Nanning, Guangxi Zhuang Autonomous Region, 530007, People's Republic of China; [2]General Surgery, The Second Affiliated Hospital of Guangxi Medical University, Nanning, Guangxi Zhuang Autonomous Region, 530007, People's Republic of China; [3]Department of Microbiology, School of Basic Medical Sciences, Guangxi Medical University, Nanning, Guangxi Zhuang Autonomous Region, 530021, People's Republic of China; [4]Department of Pain Medicine, The Second Affiliated Hospital of Guangxi Medical University, Nanning, Guangxi Zhuang Autonomous Region, 530007, People's Republic of China

*These authors contributed equally to this work

Correspondence: Juanjuan Huang, Department of Microbiology, School of Basic Medical Sciences, Guangxi Medical University, Nanning, Guangxi Zhuang Autonomous Region, 530021, People's Republic of China, Email hjjcbw@163.com; Zongbin Jiang, Department of Pain Medicine, The Second Affiliated Hospital of Guangxi Medical University, Nanning, Guangxi Zhuang Autonomous Region, 530007, People's Republic of China, Email jiangzongbin@sr.gxmu.edu.cn

Purpose: Intestinal ischemia-reperfusion injury (IIRI) occurs as a result of temporary blood flow interruption, leading to tissue damage upon reperfusion. Oxidative stress plays a critical role in this process, instigating inflammation and cell death. Identifying and characterizing genes associated with the oxidative stress response can offer valuable insights into potential therapeutic targets for managing IIRI.

Patients and Methods: The IIRI dataset was sourced from the NCBI Gene Expression Omnibus Database (GEO), while oxidative stress genes were obtained from the Genecards database. Following the acquisition of differentially expressed genes in IIRI, they were cross-linked with oxidative stress genes to yield IIRI oxidative stress related genes (IOSRGs). The least absolute shrinkage and selection operator, as well as the support vector machine with random forest algorithm, were utilized for machine learning. Subsequently, the PPI network was established, and the Degree and MNC algorithms of the Cytohuba plugin were integrated with the genes obtained through the machine learning algorithms to identify hub IOSRGs (HIOSRGs). A mouse IIRI model and ROC curve were employed to verify the accuracy of HIOSRGs. Finally, siRNA was utilized to suppress the expression of HDAC3 in Caco2 cells, and the changes in oxidative stress levels before and after hypoxia-reoxygenation in Caco2 cells were observed.

Results: A total of 277 OSRGs and 4 HIOSRGs were obtained. Concurrently, in vivo experimental results of IIRI in C57BL/6 mice, and the establishment of ROC curves, reflected the accuracy and specificity of HIOSRGs. The knockdown of HDAC3 in Caco2 cells resulted in increased oxidative stress levels before and after hypoxia-reoxygenation, underscoring the significant role of HDAC3 in IIRI.

Conclusion: This study elucidates the interplay between oxidative stress genes and IIRI, offering novel insights into the potential pathogenesis of IIRI and medical interventions for IIRI.

Keywords: IIRI, bioinformatics, potential targets, early diagnosis

Introduction

Intestinal ischemia-reperfusion injury (IIRI) is a severe condition that profoundly impacts digestive health. Its pathogenesis is multifaceted, treatment options are limited, and it frequently gives rise to severe complications, resulting in a mortality rate ranging from 50% to 90%.[1,2] Clinically, IIRI often arises from surgical procedures, vascular diseases, or other underlying causes, and in severe instances, it can culminate in grave outcomes such as intestinal tissue necrosis and multiple organ dysfunction syndrome.[3] While IIRI is associated with high mortality and complication rates, timely diagnosis can often reverse these conditions.[4,5] However, current treatment strategies for IIRI, including pharmacological preconditioning (such as anti-inflammatory treatments, apoptosis inhibitors and immune response modulators), ischemic preconditioning, and mesenchymal stem cell therapies, often fail to effectively alleviate tissue damage and restore normal function.[6–8] Given the limitations of current treatment options and the high mortality and complication rates associated with IIRI, there is an urgent need to identify new therapeutic targets for more effective intervention.

Increasing evidence suggests that oxidative stress plays a crucial role in IIRI, leading to intestinal damage and exacerbating inflammatory responses.[9–12] These oxidative stress genes encompass those involved in the regulation of cellular oxidative status and antioxidant defense systems, and their aberrant expression may precipitate elevated intracellular oxidative stress levels, thus triggering cellular damage and inflammatory reactions.[13–16] A thorough exploration of the mechanisms of action and regulatory network of oxidative stress genes in IIRI will facilitate the elucidation of the disease's pathogenesis and provide a vital theoretical foundation for the research and development of relevant treatment strategies.

High-throughput sequencing technology has revolutionized the field of gene expression analysis, enabling comprehensive and sensitive detection of gene expression changes. This technology plays a pivotal role in identifying key genes and their functions related to diseases, offering valuable insights into potential targets for disease treatment.[17–20] Given the crucial role of oxidative stress genes in IIRI, we aimed to bridge the gap between research and clinical practice.

To achieve this, we utilized the publicly available human jejunal tissue dataset before and after Whipple surgery obtained from the GEO database. Through an analysis of differentially expressed genes (DEGs) and the application of the PPI algorithm, LASSO algorithm, and SVM-RFE algorithm, in combination with oxidative stress genes sourced from the Genecards database, we identified the most critical oxidative stress genes associated with IIRI. Furthermore, we constructed an IIRI mouse model using C57BL/6 mice and subjected the intestinal tissue to immunohistochemistry analysis and PCR treatments, which corroborated our predictions.

Among the identified oxidative stress genes, we recognized HDAC3 as a key player in the context of IIRI. HDAC3 plays a crucial role in regulating mitochondrial function and oxidative stress responses. Research indicates that HDAC3 shapes the mitochondrial adaptations necessary for IL-1β production in macrophages through non-histone deacetylation.[21] Additionally, HDAC3 influences mitochondrial quality control indirectly by promoting the transcription of ROCK1.[22] However, the specific mechanisms by which HDAC3 acts in IIRI remain unclear. Therefore, we established an HDAC3 siRNA model using the CaCO2 cell line. Our experimental results demonstrated that knocking down HDAC3 exacerbated mitochondrial dysfunction and increased oxidative stress levels, thereby presenting potential therapeutic targets for future IIRI treatments. These research findings hold significant implications for a deeper understanding of the pathogenesis of IIRI and provide robust evidence for the development of novel treatment strategies.

Materials and Methods

Acquisition of IIRI Dataset

The dataset for IIRI was obtained from the publicly available GEO database. Specifically, we selected the GSE37013 dataset, which involved ischemia-reperfusion for 30 minutes, as the primary source for analyzing DEGs related to IIRI. Additionally, we utilized the GSE37013 dataset with ischemia-reperfusion for 120 minutes to identify selected key genes over a longer duration. The detailed information of the GSE37013 dataset is summarized in Table 1.

Acquisition of DEGs

To convert the "ID-REF" format of the GSE37013 dataset, we used GPL platform files to map it to the corresponding "Gene symbol". Subsequently, the R software (version 4.4.1) package "limma" was employed to perform linear model

Table 1 Data Set Information

Accession	Platforms	Sample Source	Control Group	IIRI Group
GSE37013-30min	GPL6947	jejunum	7	7
GSE37013-120min				7

fitting and differential analysis on the sorted matrix file by averaging multiple gene probes associated with the same gene symbol.[23,24] We set a screening criterion of P value<0.05 to ensure the identification of DEGs with biological significance. Additionally, the ggplot2 package was used to generate principal component analysis (PCA) plots.

Construction of Protein-Protein Interaction Network

The top 2000 genes, ranked by their significance, were imported into the STRING database to construct a protein-protein interaction network. Subsequently, the obtained table was imported into Cytoscape software for visualization and analysis. The Degree and MNC algorithms of the CytoHubba plugin were employed to identify key genes within the network.[25,26]

Acquisition of Oxidative Stress Genes and IOSRGs

The Genecards website (https://www.genecards.org/) was utilized to obtain genes associated with oxidative stress. A keyword search using "oxidative stress" was performed, and genes with a relevance score<5 were excluded to ensure the selection of highly correlated genes.[27,28] The DEGs obtained previously were then intersected with the oxidative stress genes, resulting in the identification of the retained IOSRGs.

GO and KEGG Enrichment Analysis

To gain deeper insights into the critical role of IOSRGs in IIRI, we performed functional enrichment analysis and GO/ KEGG enrichment analysis on the gene sets using the "clusterProfiler" package. The results of the enrichment analyses were then visualized utilizing the "enrichplot" package.

LASSO and SVM-RFE

To further identify the most critical IOSRGs, the LASSO regression and SVM-RFE algorithms were employed.[29,30] Specifically, the glmnet package was utilized for LASSO regression analysis. Coefficient path diagrams were generated under different penalty lambda levels to determine the optimal lambda value. Cross-validation was then performed using the cv.glmnet function to select the optimal lambda value and its corresponding coefficients. The LASSO algorithm was used to select genes with important features.

Subsequently, the SVM-RFE algorithm was employed for feature selection. The implementation of this algorithm relied on the e1071 packages in the R language. The SVM functions were utilized to construct a support vector machine model, and the feature selection process was optimized recursively. Multiple subsampling was supported by setting the parameter k to enhance the stability of feature weights. To avoid overfitting, strict separation of training and test data was maintained during the feature selection process to ensure fair model evaluation. Finally, the key genes were identified.

Acquisition of HIOSRGs

The key genes identified through the Degree, MNC algorithm, LASSO, and SVM-RFE algorithms were consolidated and subjected to further analysis. Genes that were co-expressed across all four methodologies were subsequently recognized as the final set of highly significant HIOSRGs. Future validation studies will be conducted to further investigate the relevance of these HIOSRGs.

 703

Establishment of ROC Curve

The Receiver Operating Characteristic (ROC) curve is a valuable tool for assessing the performance of binary classification models. To evaluate the diagnostic performance of the four HIOSRGs in identifying IIRI, ROC curves were constructed utilizing the pROC package.[31,32]

Immune Infiltration Analysis

The CIBERSORT function was utilized for analyzing the cellular components within each dataset, and cyclic processing of immune cell data was carried out using the Pacman package. The correlation between each target gene and immune cell was computed, and correlation scatter plots were generated.[31,33] A significant correlation (p-value < 0.05) between the target gene and each immune cell, after adjusting for multiple comparisons, was considered indicative of an association between the target gene and the respective immune cell.

Establishment of miRNA-mRNA Interaction Network

The Network Analyst database (https://www.networkanalyst.ca/) was utilized to construct a miRNA-mRNA interaction network.[34] Four HIOSRGs were incorporated into the gene list for analysis. The organism was specified as Homo sapiens (human), and the Official Gene Symbols were selected as the Set ID type. For the network interaction analysis, TarBase v9.0 was chosen, and the resulting interaction network was imported into Cytoscape software for visualization.

PCR

For the DNA samples extracted from intestinal tissue, reverse transcription reagents from Vazyme Biotech (China) were utilized. Gene primers were prepared as outlined in Table 2. The extracted DNA, gene primers, and qPCR Master Mix were then subjected to PCR amplification using a predetermined temperature cycling protocol.

Animal and IIRI Models

C57BL/6 male mice (8–10 weeks old, 22–25g) were obtained from the Animal Center of Guangxi Medical University. The mice were housed in specific pathogen-free (SPF) rooms with a 12-hour light-dark cycle and provided with ad libitum access to clean water and food. The experimental procedures followed the ARRIVE guidelines (https://arrivalguidelines.org).

Prior to the experiment, the mice were fasted for 12 hours while having free access to water. The mice were then randomly allocated into two groups: the intestinal ischemia-reperfusion group (IIRI group) and the Sham group. In the IIRI group, mice were intraperitoneally anesthetized with 1% pentobarbital (50mg/kg) and subjected to surgical procedures involving clamping and subsequent release of the superior mesenteric artery (SMA) to induce ischemia and reperfusion. The SMA in the IIRI group was occluded for a duration of 45 minutes. Specimens were collected after 30 minutes of reperfusion to establish the IIRI model. The Sham group underwent the same procedure without arterial clamping. Subsequently, the mice were euthanized using cervical dislocation.

Table 2 Primer Sequences Used for HIOSRGs

Gene	Primer
ALDH18A1-mus	GTGATCTTCAGGGGGTAAATGTGA
	TTGCATCATCTGAGCCTGGG
ABCG2-mus	GGAGGCAAGTCTTCGTTGC
	GTGCCCATCACAACGTCATC
CYP1A2-mus	ACAGCAAGGACTTTGTGGAGAA
	GTGATGTCTTGGATACTGTTCTTGT
HDAC3-mus	TCGAGGACATGGGGAATGTG
	TGGAGTGTGAAATCTGGGGC
HDAC3-hsa	GTGCATTGTGCTCCAGTGTG
	CTACCAGCAGCGATGTCTCA

Hematoxylin and Eosin Staining

Tissue samples from the mouse intestines were subjected to sampling, fixation, dehydration, embedding, and staining procedures, followed by visualization and imaging using an optical microscope. For detailed steps, please refer to the supplementary - materials and methods.

Apoptosis Detection

Tissue samples from the mouse intestines were subjected to sampling, fixation, dehydration, embedding, and sectioning processes. The TUNEL cell apoptosis detection kit (Beyotime, China) was utilized to stain the intestinal tissue, and imaging was conducted using a fluorescence microscope. Detailed procedures can be found in the supplementary - materials and methods.

Immunohistochemistry

Tissue samples from the mouse intestine underwent sampling, fixation, dehydration, embedding, sectioning, antigen retrieval, primary antibody treatment, and secondary antibody treatment. The captured images were obtained using an optical microscope. The positive stained area of each immunohistochemical image was measured and quantified using ImageJ software. The specific antibodies used are detailed in Table 3.

Caco2 Cell Culture

Caco2 cells were procured from the Affiliated Cancer Hospital of Guangxi Medical University. The cells were cultured in 80% DMEM medium (containing non-essential amino acids), 20% fetal bovine serum, and appropriate concentrations of penicillin and streptomycin. The cells were maintained in an incubator at 5% CO_2 and 37°C.

siRNA Transfection

For further investigation of HIOSRGs, lipofectamine 3000 (Invitrogen, Carlsbad, CA, USA) was utilized to transfect HDAC3 siRNA and control siRNA into Caco2 cells for 12 hours. Subsequently, the medium was replaced with fresh culture medium. After 48 hours of cultivation, the cells were divided into groups to establish the model. The siRNA double-stranded body was synthesized by NanningGenSysbiotechnology Co., Ltd. (Nanning, China), and the sequences are as follows:

HDAC3-siRNA: 5'-3': CGCAUCGAGAAUCAGAACUCA, UGAGUUCUGAUUCUCGAUGCG
Control siRNA: 5'-3': UUCUCCGAACGUGUCACGU, ACGUGACACGUUCGGAGAA.

Establishment of in vitro H/R Model

To further investigate the HIOSRGs, an in vitro hypoxia/reoxygenation (H/R) model was established. The cells were divided into four groups as follows:

Sham+siNC group: Caco2 cells transfected with control siRNA were cultured in an air incubator with 21% O_2, 5% CO_2, and a temperature of 37°C for growth.

H/R+siNC group: Caco2 cells transfected with control siRNA were exposed to an air incubator with <0.5% O_2, 2.0% CO_2, and a temperature of 37°C for 12 hours, followed by 6 hours of reoxygenation.

Sham+si HDAC3 group: Caco2 cells transfected with si HDAC3 were cultured in an air incubator with 21% O_2, 5% CO_2, and a temperature of 37°C.

Table 3 The Antibodies for HIOSRGs

Gene	Cat No
ALDH18A1	17719-1-AP, proteintech group, 1:100
ABCG2	27286-1-AP, proteintech group, 1:100
CYP1A2	19936-1-AP, proteintech group, 1:100
HDAC3	10255-1-AP, proteintech group, 1:100

 705

H/R+si HDAC3 group: Caco2 cells transfected with si HDAC3 were exposed to an air incubator with <0.5% O2, 2.0% CO2, and a temperature of 37°C for 12 hours, followed by 6 hours of reoxygenation.

Reactive Oxygen Species Detection

Caco2 cells cultured in a six-well plate were treated according to the instructions provided with the reactive oxygen species detection kit (Beyotime, China). Briefly, the cells were incubated with DCFH-DA at a final concentration of 10 micromoles per liter for 20 minutes, after which they were observed under a fluorescence microscope.

Mitochondrial Membrane Potential Detection

Caco2 cells cultured in a six-well plate were treated according to the instructions provided with the mitochondrial membrane potential detection kit (Beyotime, China). In brief, the cells were incubated with an appropriate concentration of JC-1 staining solution for 20 minutes, after which they were observed using a fluorescence microscope.

MitoSOX Detection

Caco2 cells cultured in a six-well plate were treated according to the instructions provided with the mitochondrial superoxide detection kit (Beyotime, China). Briefly, the cells were incubated with a 5 μM staining solution for 20 minutes, after which they were analyzed using a fluorescence microscope.

Statistical Analysis

Statistical analysis was carried out using GraphPad Prism 9 software. All data are presented as mean ± standard deviation. *T*-tests were used to compare two groups, while one-way analysis of variance (ANOVA) followed by Dunnett's test was used to analyze differences among four groups. In the statistical analysis, $*p<0.05$, $**p<0.01$, and $***p<0.001$ were considered statistically significant.

Results

Differential Expression Analysis

The study's flowchart is presented in Figure 1, and the PCA analysis is detailed in Supplementary Figure 1. The gene expression box plot in Figure 2A illustrates the consistent distribution of expression data in the GSE37013 dataset, validating its suitability for analysis. Notably, a total of 2638 DEGs were identified, comprising 1170 upregulated genes and 1468 downregulated genes (Figure 2B). Furthermore, the heatmap in Figure 2C showcases the top 50 genes with significant differences.

Acquisition of IOSRGs and GO KEGG Enrichment Analysis

Intersection of the aforementioned DEGs with oxidative stress genes yielded 277 IOSRGs (Figure 3A), which were subsequently subjected to enrichment analysis (Figure 3B and C). Intriguingly, the Gene Ontology enrichment with IOSRGs highlighted biological processes primarily associated with responses to oxidative stress and cellular reactions to oxidative stress. Regarding cellular components, enrichment was observed in the mitochondrial inner membrane, while molecular functions were predominantly enriched in oxidative activity. Additionally, the Kyoto Encyclopedia of Genes and Genomes enriched pathways related to oxidative stress, including the MAPK signaling pathway, PI3K-Akt signaling pathway, and Chemical carcinogenesis - reactive oxygen species. Given the strong association between mitochondrial function and oxidative stress, alongside the enrichment of IOSRGs in pathways related to mitochondrial function, these findings provide robust theoretical support for our in-depth investigation of IOSRGs and mitochondrial oxidative stress levels.

Acquisition of HIOSRGs

The acquired DEGs were input into the STRING database to construct a protein-protein interaction network, and subsequently imported into Cytoscape software. By utilizing the MNC algorithm and Degree algorithm of the
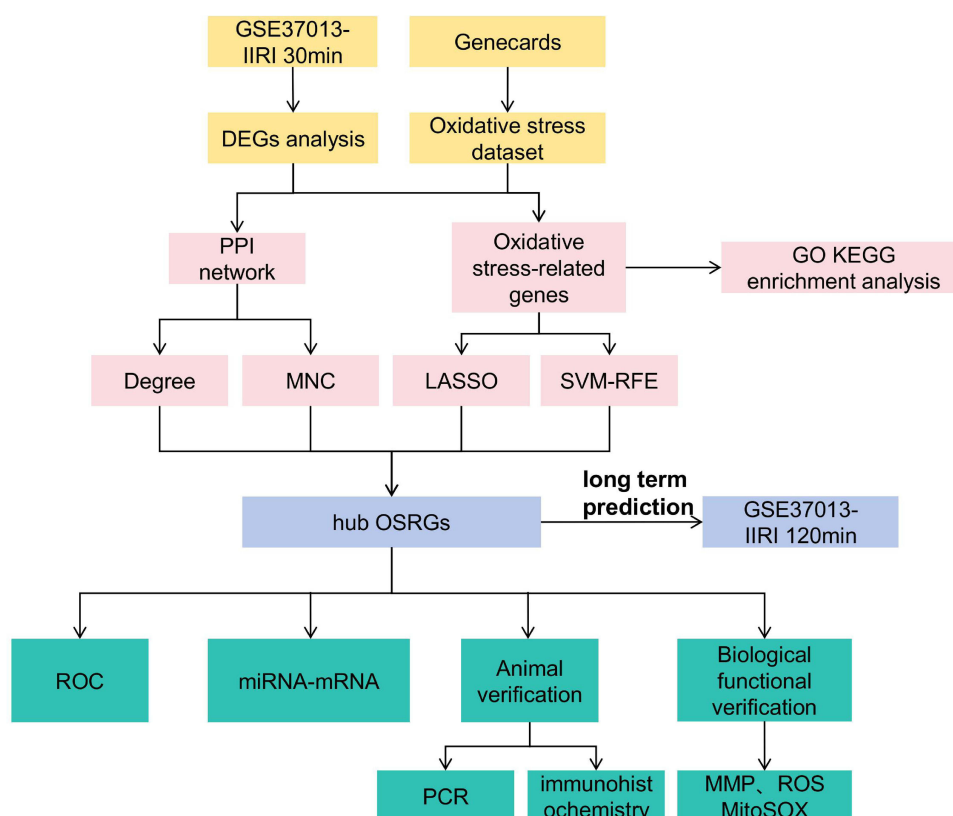
Figure 1 Research flowchart.

CytoHubba plugin, the top 200 genes (TOP10%) were calculated (Figure 4A and B). Following this, we employed LASSO and SVM-RFE to screen IOSRGs, yielding 8 and 43 key genes, respectively (Figure 4C-E). Ultimately, the genes obtained from the four algorithms were merged (Figure 4F), resulting in the identification of four HIOSRGs: ALDH18A1, ABCG2, CYP1A2, and HDAC3.

ROC Analysis

To elucidate the expression trends and diagnostic efficacy of HIOSRGs in IIRI, gene heatmaps were constructed (Figure 5A), and ROC plots were generated (Figure 5B-E). Encouragingly, all four HIOSRGs exhibited favorable diagnostic performance, further reinforcing the direction of our research.

Immune Infiltration Analysis

Considering the well-documented relationship between oxidative stress and immune responses, we created correlation maps (Figure 6A-D) to explore the association between HIOSRGs and immune infiltrating cells, utilizing the correlation expression matrix from GSE37013. The results demonstrated positive correlations between ABCG2 and T cell gamma delta, ALDH18A1 and Mast cell resting, CYP1A2 and B cell naive, HDAC3 and T cell CD4 memory activated in IIRI. This provides valuable insight for our future research into the impact of HIOSRGs on immune function in IIRI.

Animal in vivo Validation

Subsequently, an IIRI animal model was established, and histological examination (HE results in Figure 7A) revealed mucosal damage, disruption of the mucosal barrier, and inflammatory cell exudation in the intestinal tissue of mice subjected to IIRI (indicated by red arrows). TUNEL staining showed an increase in apoptotic cells in the intestinal tissue of IIRI mice (Figure 7B), validating the successful construction of the IIRI model. Subsequent PCR and immunohistochemistry analyses of HIOSRGs demonstrated an increasing trend in ABCG2 and ALDH18A1, and a decreasing trend in CYP1A2 and HDAC3 in the intestinal
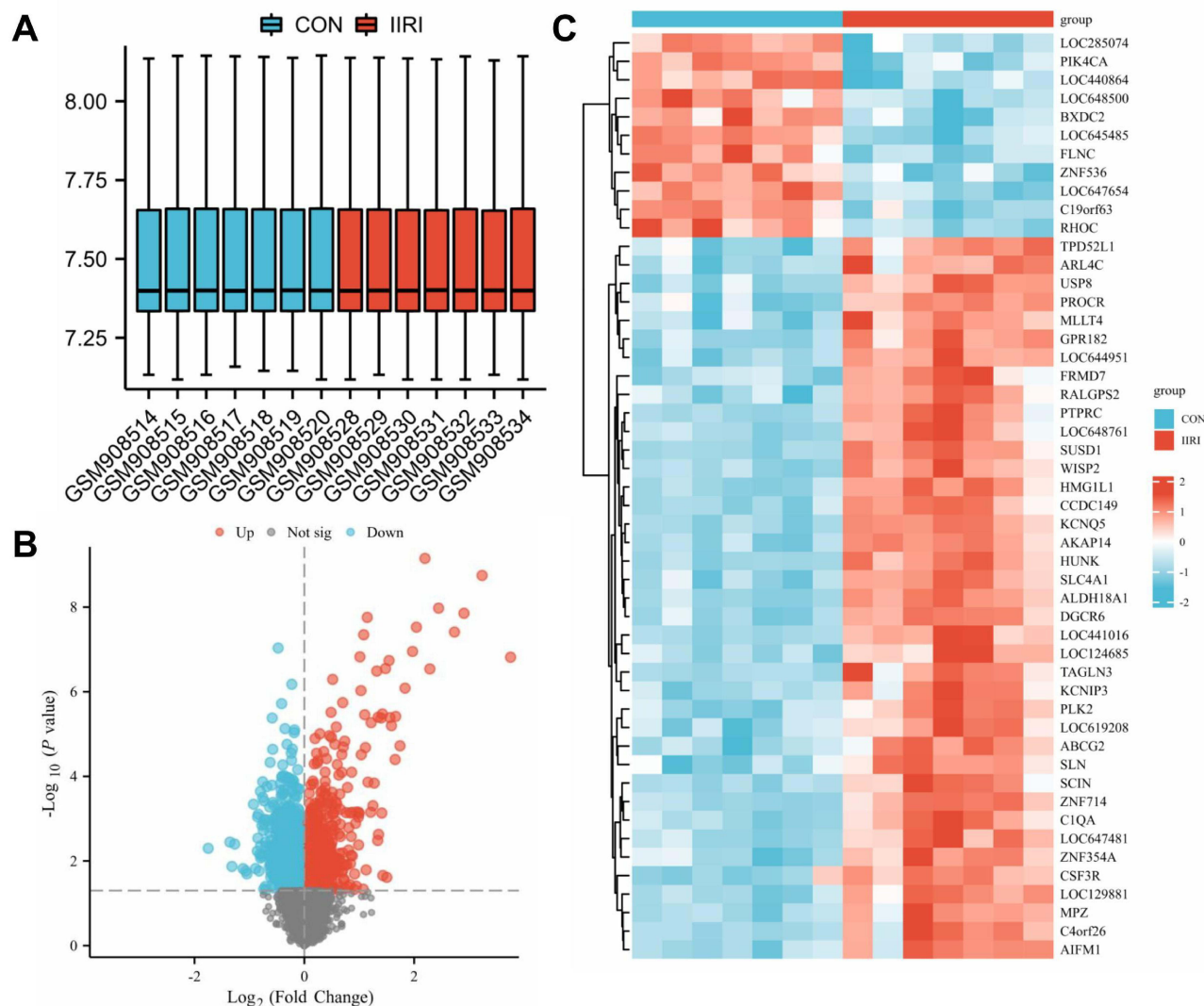
Figure 2 Acquisition of DEGs. (**A**) Box plot illustrating expression levels for the IIRI dataset. (**B**) Volcano plot depicting DEGs. The red dots represent upregulated genes, the blue dots represent downregulated genes, and the gray dots represent non-significant genes. (**C**) Heatmap displaying expression levels of DEGs.

tissue of IIRI mice compared to Sham group mice (Figure 7C-N) (Figure 8A-D), thereby affirming the reliability of HIOSRGs through in vivo experiments.

Construction of miRNA-mRNA Network

MiRNAs play pivotal roles in cellular biological functions by regulating gene expression. Their significance lies in their ability to bind to the mRNA of target genes, leading to mRNA degradation or translation inhibition, thus regulating gene expression. To understand the miRNAs regulating HIOSRGs, we constructed a miRNA-mRNA network by utilizing the Network Analyst Database (Figure 9). This network comprises 4 hIOSRGs and 241 miRNAs, encompassing a total of 350 regulatory relationships. This framework provides a useful tool for researchers to further investigate miRNA regulatory processes.

Inhibition of HDAC3 Expression Exacerbates H/R-Induced Oxidative Stress and Mitochondrial Dysfunction

We conducted siHDAC3 transfection in Caco2 cells and confirmed successful transfection via PCR (Figure 10A). The results revealed that inhibiting HDAC3 expression increased ROS and mitoROS induced by IIRI (Figure 10B-E) and
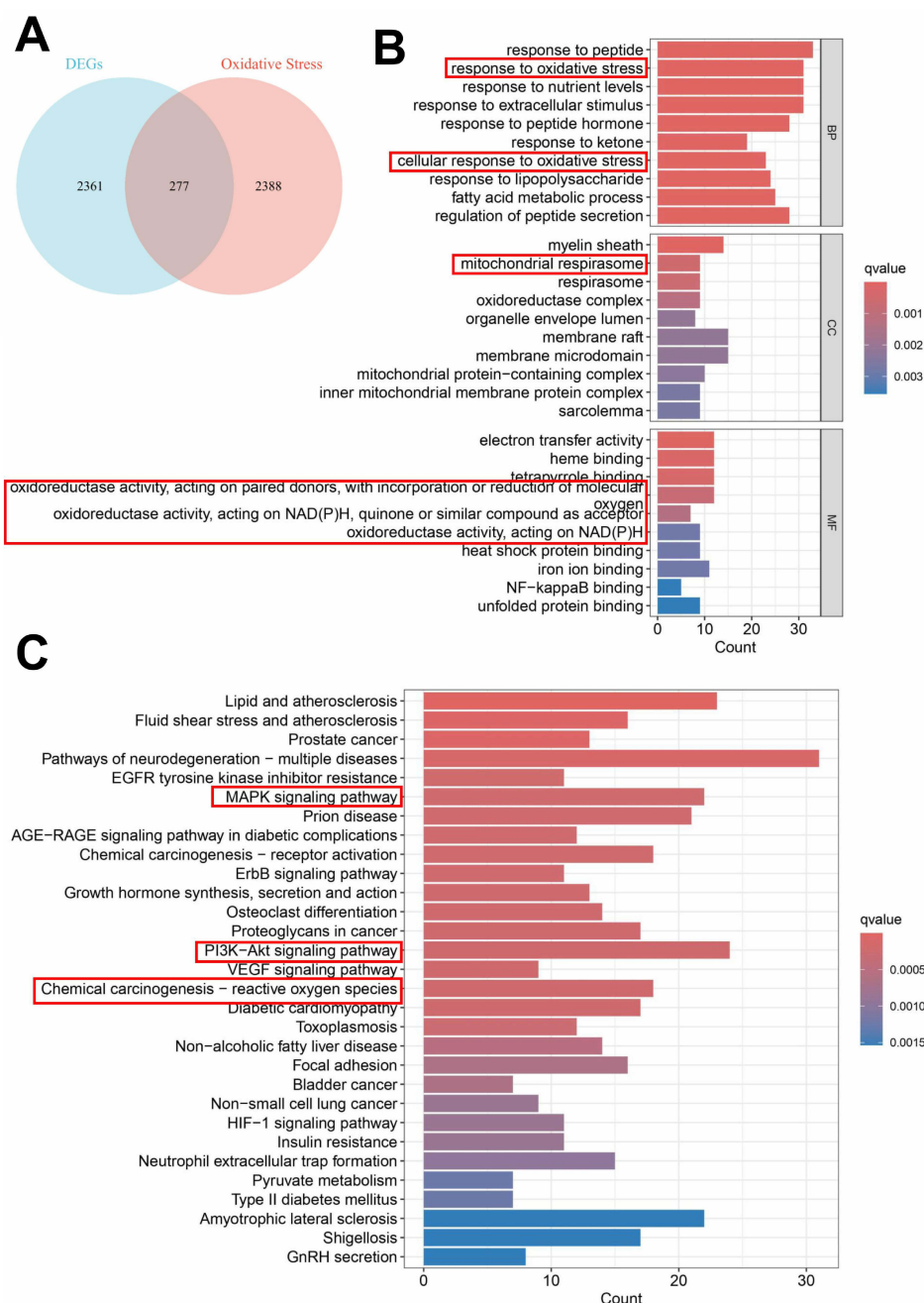
Figure 3 Acquisition of IOSRGs and GO KEGG enrichment analysis. (**A**) Venn diagram illustrating the overlap between DEGs and oxidative stress genes. (**B**) GO analysis of IOSRGs. (**C**) KEGG enrichment analysis of IOSRGs.

decreased mitochondrial membrane potential levels (Figure 10F-G). These findings indicate that the absence of the oxidative stress gene HDAC3 exacerbates mitochondrial dysfunction and the oxidative stress state induced by H/R. This provides compelling support for our future research on HDAC3 as a key gene in IIRI oxidative stress.

Long-Term Forecast of HIOSRGs

To ascertain whether the trend of HIOSRGs changes at extended time points aligns with that observed at 30 minutes, we compiled the expression matrix of HIOSRGs following 4 hours of IIRI in GSE37013. Through bioinformatics analysis, we obtained insights into the expression patterns and trends associated with these genes. As anticipated, the trend of
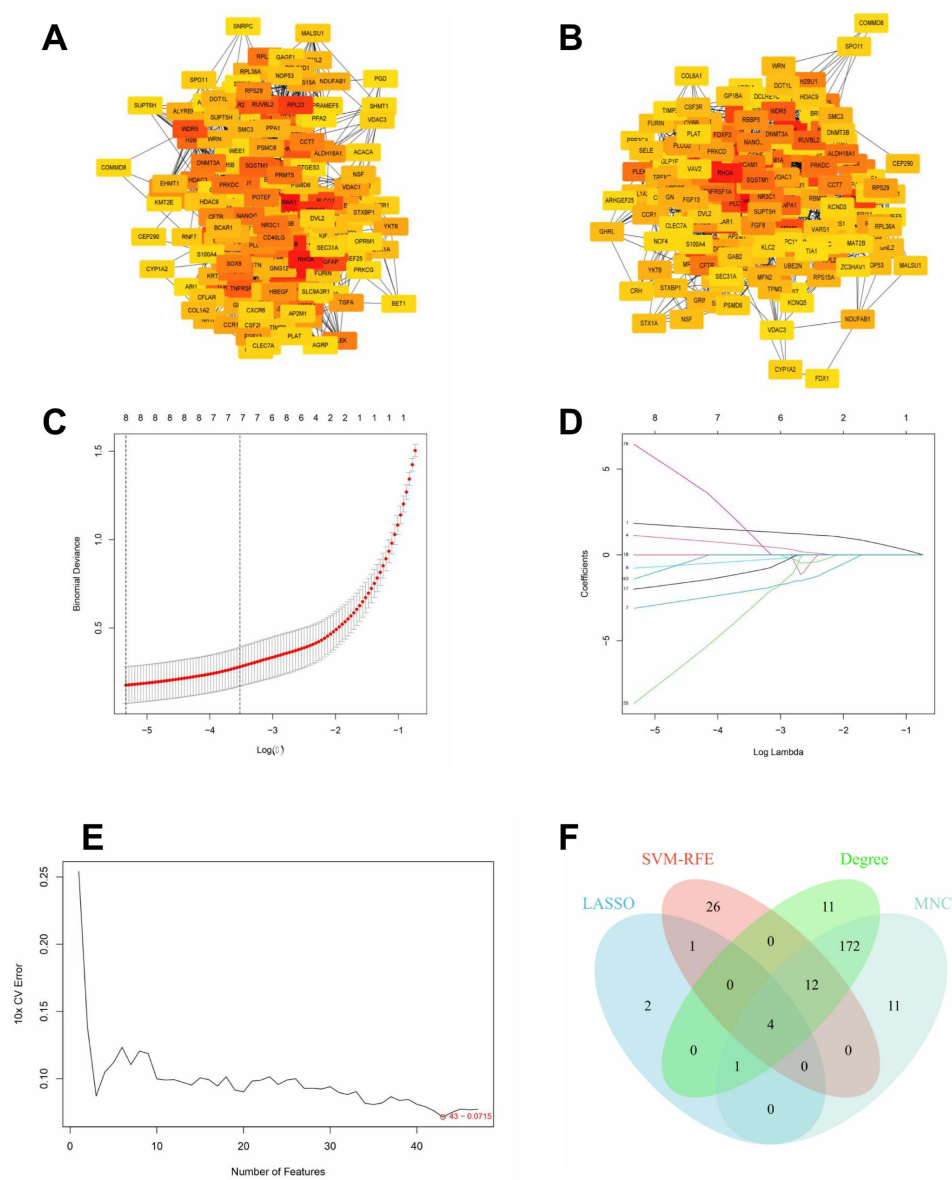
Figure 4 Acquisition of 4 hIOSRGs. (**A** and **B**) Top 10% genes identified by MNC and Degree algorithms using the cytohubba plugin. (**C** and **D**) Minimum and lambda graphs generated by LASSO machine learning. (**E**) Support Vector Machine (SVM) graph generated by SVM-RFE machine learning. (**F**) Venn diagrams displaying the overlap between MNC, Degree algorithm, LASSO, and SVM-RFE machine learning algorithms.

changes in the four HIOSRGs remained consistent with the 30-minute time point (Figure 11A-D), thereby reinforcing the necessity of our experiment.

Discussion

Intestinal ischemia-reperfusion injury (IIRI) is a severe condition characterized by tissue damage upon the restoration of blood supply after intestinal ischemia. Prompt detection and treatment of IIRI are crucial for patient prognosis, as the condition can lead to intestinal necrosis and life-threatening situations. Ischemia deprives tissue cells of oxygen and nutrients, resulting in cellular damage. Upon reperfusion, oxidative stress occurs as the production of reactive oxygen species and other oxidants exceeds the cell's clearance capacity. This leads to lipid peroxidation, protein oxidation, DNA damage, and further exacerbates tissue injury. Understanding the changes in oxidative stress genes in IIRI is essential for studying the underlying mechanisms.
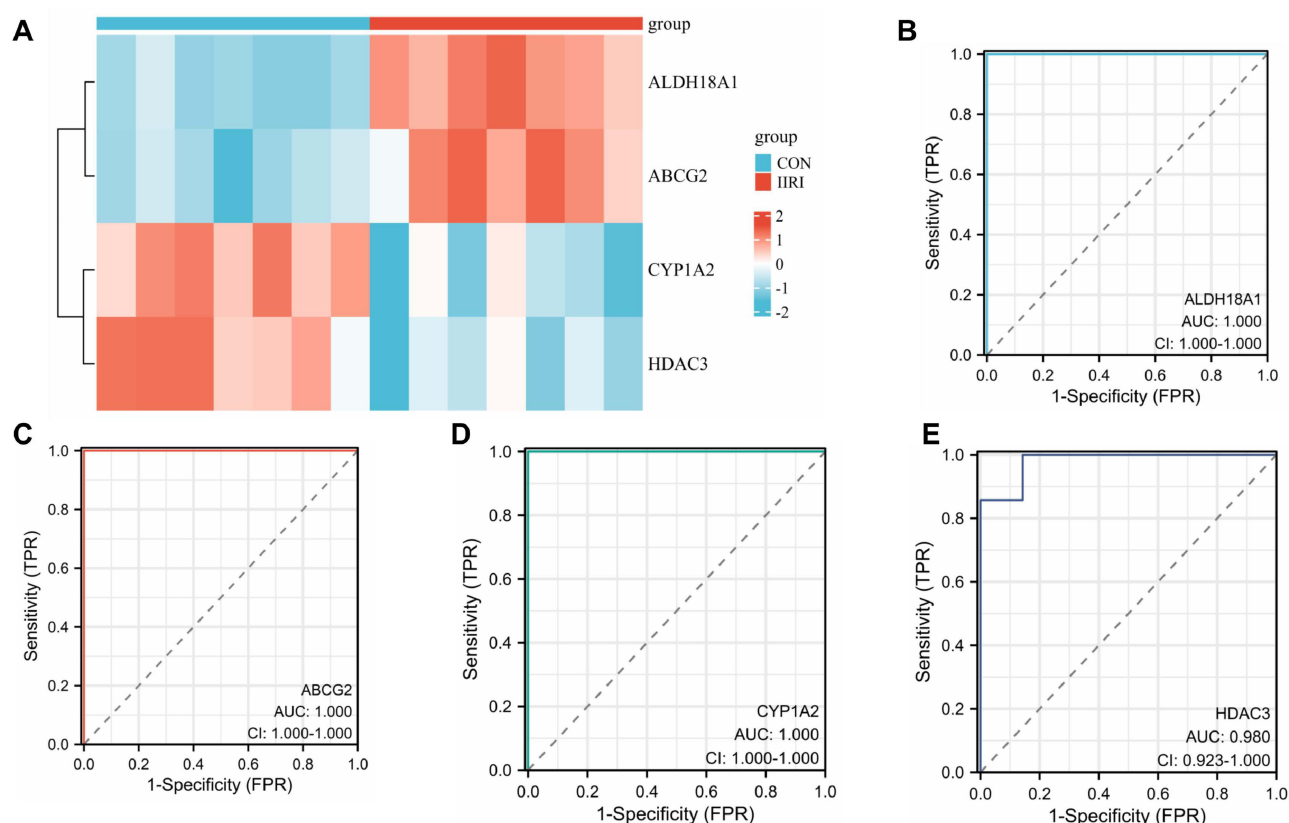
Figure 5 Heatmaps and ROC curves of expression levels of four HIOSRGs. (**A**) Heatmap illustrating expression levels of the 4 hIOSRGs. (**B-E**) ROC curves demonstrating the performance of ALDH18A1, ABCG2, CYP1A2, and HDAC3.

In this study, we conducted bioinformatics analysis to explore the alterations in oxidative stress genes in IIRI. Initially, we identified 2638 genes that exhibited significant changes, including 1170 upregulated genes and 1468 downregulated genes. To gain a deeper understanding of these changes, we performed an intersection analysis between the DEGs and oxidative stress genes, resulting in the identification of 277 IOSRGs. Gene Ontology enrichment analysis revealed that these IOSRGs were mainly associated with biological processes related to oxidative stress and cellular response to oxidative stress. In terms of cellular components, the mitochondrial inner membrane was significantly enriched, while oxidoreductase activity was the predominant molecular function. Furthermore, the Kyoto Encyclopedia of Genes and Genomes revealed significant enrichment of pathways related to oxidative stress, such as the MAPK signaling pathway, PI3K-Akt signaling pathway, and Chemical carcinogenesis - reactive oxygen species. These findings are remarkable, as they indicate that oxidative stress plays a critical role in IIRI and is intricately involved in mitochondrial function. Consequently, this provides a solid theoretical foundation for our subsequent exploration of HDAC3 knockdown and the investigation of mitochondrial functional status.

In our pursuit of identifying crucial oxidative stress genes, we employed the MNC algorithm, Degree algorithm, and machine learning techniques such as LASSO and SVM-RFE to construct protein-protein interaction (PPI) networks. Synthesizing these results, we identified four HIOSRGs: ALDH18A1, ABCG2, CYP1A2, and HDAC3.

Subsequently, we established ROC curves for the four HIOSRGs, demonstrating their favorable diagnostic performance. Furthermore, the construction of the miRNA-mRNA network provided an initial insight into the exploration of miRNAs regulating oxidative stress genes in IIRI.

To validate the accuracy of HIOSRGs, a mouse IIRI model was established. Intestinal tissues from the Sham group and the IIRI group were collected, and immunohistochemistry staining and quantitative PCR analysis were performed. The results from both analyses substantiated the consistency of the observed trends in the four HIOSRGs with the bioinformatics predictions.
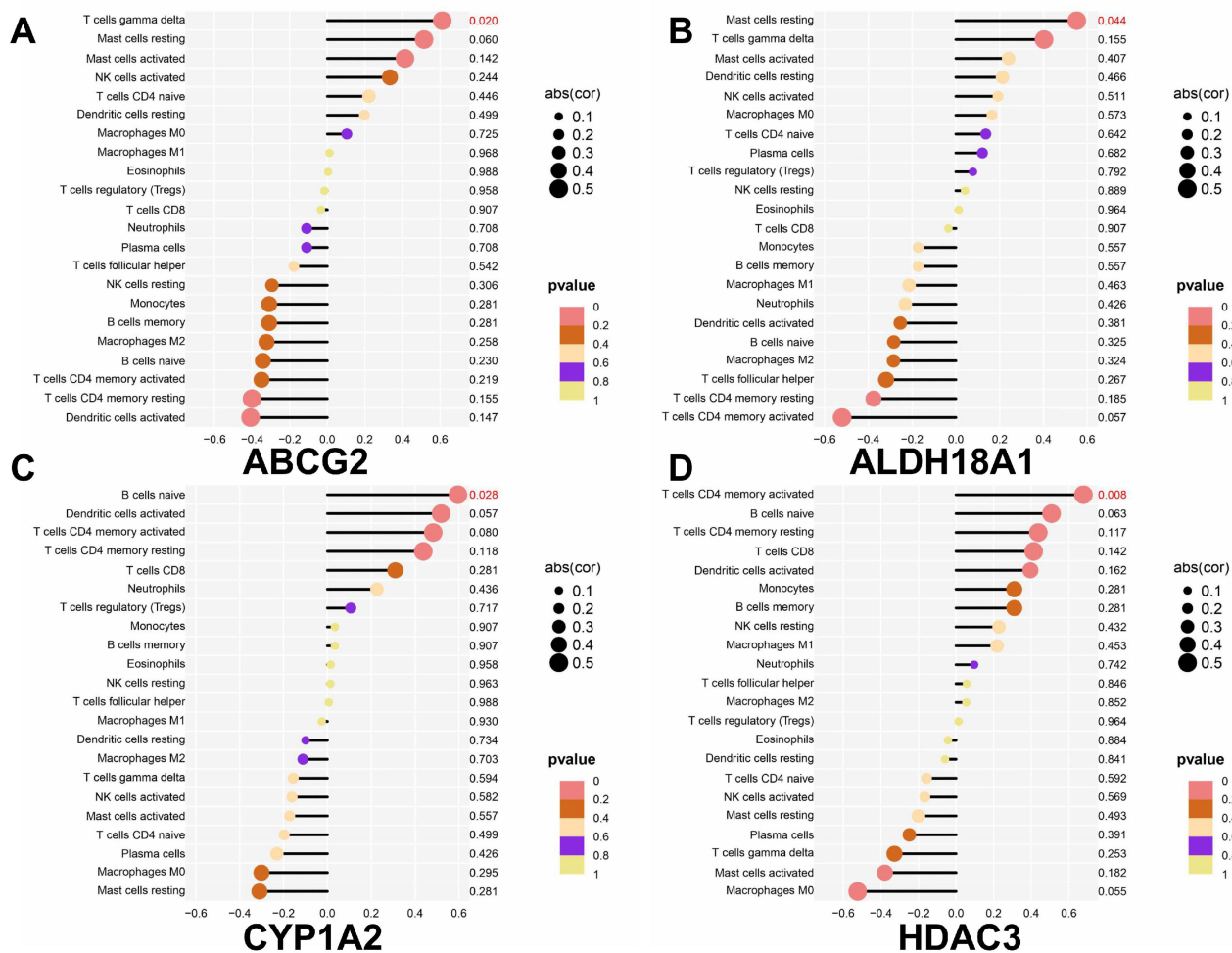
Figure 6 Correlation between 4 hIOSRGs and immune infiltrating cells. (**A-D**) Correlation maps displaying the relationship between ABCG2, ALDH18A1, CYP1A2, HDAC3, and 22 immune infiltrating cell types.

On the molecular level, the ALDH18A1 gene encodes δ-1-pyrroline-5-carboxylate synthase (P5CS),[35,36] a crucial enzyme that catalyzes the synthesis of δ-1-pyrroline-5-carboxylate (P5C), an essential intermediate product in the biosynthetic pathways of proline and arginine. Notably, the small intestine serves as the exclusive site for arginine synthesis in newborns, and low circulating arginine levels are associated with the occurrence of necrotizing enterocolitis.[37] P5CS is implicated in the metabolic pathways of proline and arginine, and the rate of proline metabolism significantly influences the regulation of intracellular reactive oxygen species (ROS) levels.[38,39] Additionally, research by Chunhua Ma et al highlighted the potential of L-arginine, an essential amino acid, as an alternative treatment for chronic obstructive pulmonary disease (COPD) by modulating the ROS/NLRP3/NF-κB signaling pathway.[40] Furthermore, Alyssa Margolis discovered that arginine metabolism enhances Salmonella resistance to oxidative stress.[41] These findings underline the crucial role of ALDH18A1 and its associated pathways in oxidative stress regulation and disease pathogenesis.

The findings of our study demonstrated an increasing trend of ALDH18A1 in IIRI. ALDH18A1 may exert a protective role in IIRI through its involvement in proline synthesis, arginine metabolism, and participation in antioxidant, anti-inflammatory, and cell apoptosis mechanisms. Further investigation into the underlying mechanism of ALDH18A1 in IIRI holds promise for providing novel insights into the treatment and prevention of this disease.

Recent research indicates that mutations in the ALDH18A1 gene can lead to decreased enzyme activity and have been associated with hereditary disorders. For example, a study on recessive hereditary spastic paraplegia identified mutations in ALDH18A1 that resulted in reduced enzyme function, underscoring the gene's importance in metabolic health and
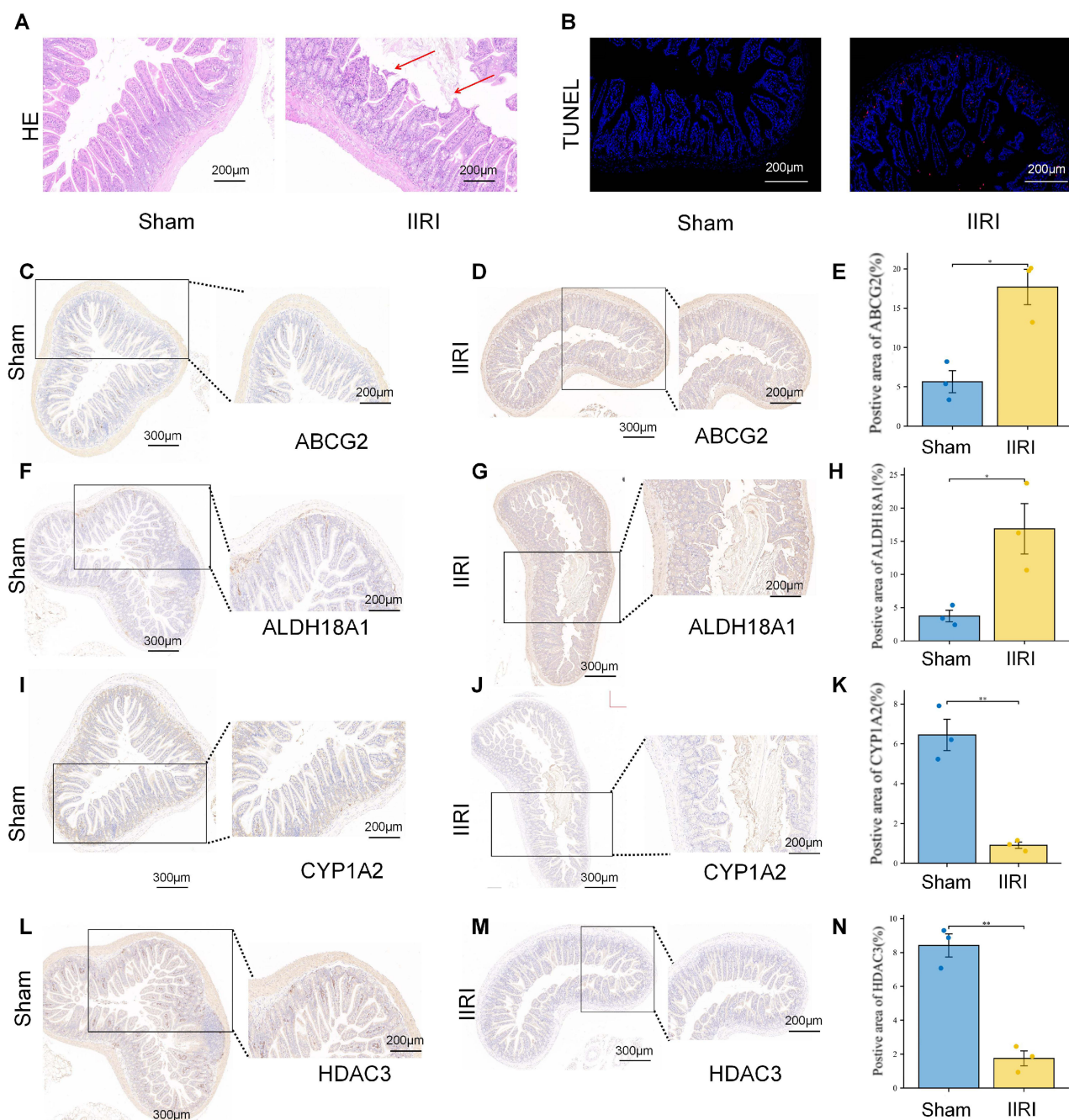
Figure 7 Successful construction of IIRI animal model and immunohistochemistry of HIOSRGs. (**A**) HE stained maps of the Sham group and IIRI group, scale=200 μm. Histological examination revealed mucosal damage, disruption of the mucosal barrier, and inflammatory cell exudation in the intestinal tissue of mice subjected to IIRI (indicated by the red arrows). (**B**) Apoptosis detection in the Sham group and IIRI group, scale bar=200 μm. (**C-N**) Immunohistochemistry maps and quantification charts of ABCG2, ALDH18A1, CYP1A2, and HDAC3 in the Sham and IIRI groups, scale=300 μm (left), scale=200 μm (right). *: P<0.05, **: P<0.01.

disease.[42] Furthermore, ALDH18A1 has been implicated in cancer metabolism. Elevated expression of ALDH18A1 in clear cell renal cell carcinoma (ccRCC) has been linked to poor prognosis, suggesting that targeting this gene could have significant therapeutic implications in oncology as well.[43] These observations highlight the versatility of ALDH18A1 as a potential target in both metabolic disorders and cancer therapies.

ABCG2, also known as breast cancer resistant protein, is an ATP-binding membrane transport protein widely expressed in various tissues and cell types, including the intestine, liver, and kidney.[44,45] As a member of the ATP Binding Cassette (ABC) transport family, ABCG2 influences the pharmacokinetics of foreign compounds, potentially
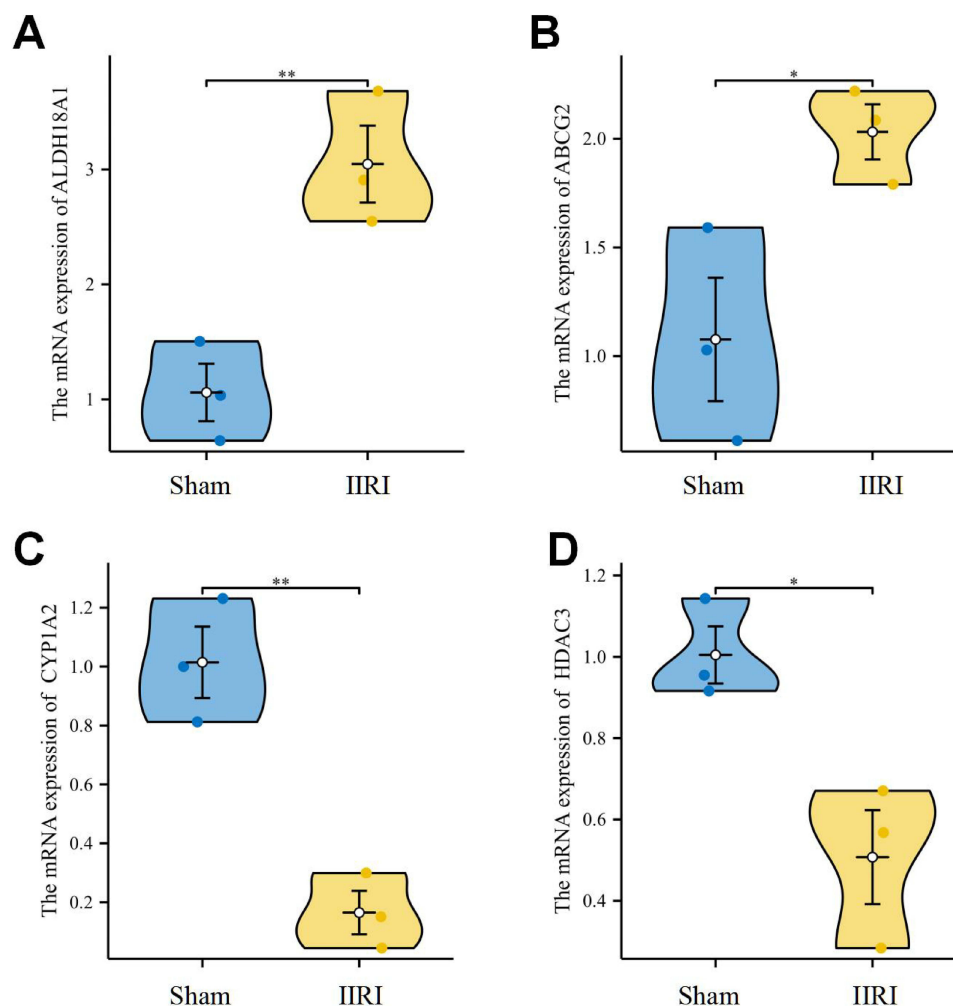
Figure 8 The mRNA expression levels of 4 hIOSRGs. (**A-D**) mRNA expression levels of ALDH18A1, ABCG2, CYP1A2, and HDAC3 in the Sham and IIRI groups. *: P<0.05, **: P<0.01.

impacting the efficacy and toxicity of numerous drugs.[46] ABCG2 exhibits dual roles in the regulation of oxidative stress levels. On one hand, the Nrf2-ABCG2 signaling pathway enhances oxidative stress levels in ovarian cancer.[47] On the other hand, ABCG2 has been shown to alleviate oxidative stress and inflammatory responses by inhibiting the NF-κB signaling pathway in colorectal cancer cell models and lung adenocarcinoma.[48,49]

In a clinical context, targeting ABCG2 could open new avenues for therapeutic intervention. For instance, pharmacological inhibitors of ABCG2 could enhance the efficacy of chemotherapeutic agents by improving their bioavailability and reducing oxidative stress-related damage. A proof-of-concept study illustrated that pharmacologic inhibition of ABCG2 can significantly enhance the delivery of drugs across the blood-brain barrier, particularly for tyrosine kinase inhibitors in brain tumor therapy.[50] This finding underscores the potential for ABCG2 inhibitors to improve drug efficacy and minimize toxic side effects in patients.

Our study identified an increasing trend of ABCG2 expression in IIRI. Elevated ABCG2 levels may enhance drug excretion, modulate oxidative stress, and influence inflammation, positioning it as a key regulatory factor and therapeutic target in IIRI.

Pharmacological inhibitors of ABCG2 could improve treatment efficacy by increasing the bioavailability of substrate drugs and aiding in the management of oxidative stress and inflammation. Developing agents to selectively modulate ABCG2 expression may optimize treatment strategies and improve patient outcomes, highlighting the need for further research on ABCG2's therapeutic potential in IIRI.

CYP1A2, a prominent cytochrome P450 (CYP) enzyme primarily found in the liver, holds substantial importance as both a drug-metabolizing enzyme and an endogenous compound-metabolizing enzyme in the human body.[51,52] It
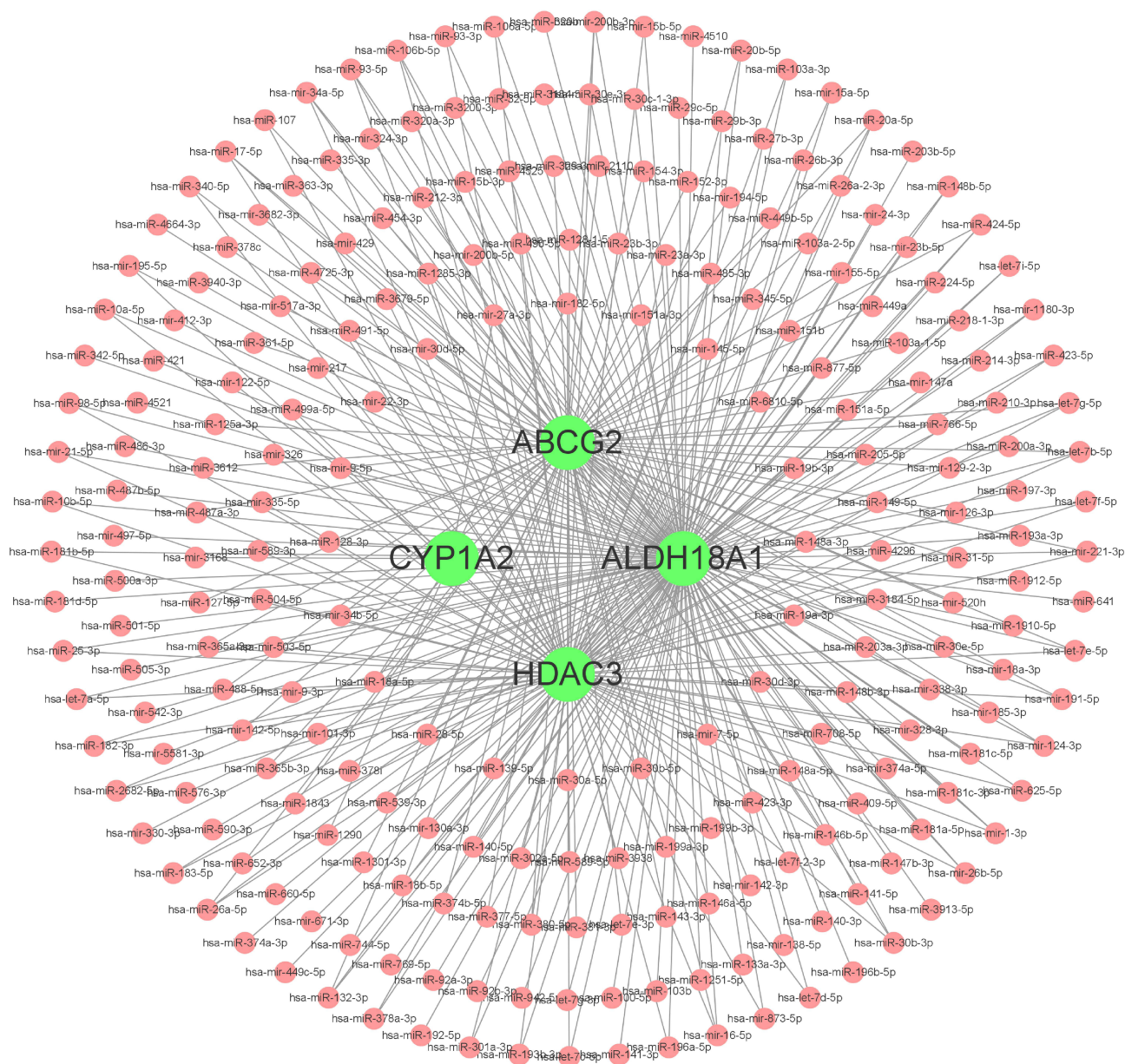
Figure 9 The miRNA-mRNA interaction diagram, illustrating the interaction network between the four HIOSRGs and their corresponding miRNAs. Green dots represent mRNA, and pink dots represent miRNA.

demonstrates functional activity in both hepatic and extrahepatic regions. In the small intestine, CYP1A2 participates in the metabolism of numerous endogenous and exogenous compounds, including drugs, environmental toxins, and dietary constituents.[53,54] Through the actions of CYP1A2, these substances can undergo conversion into metabolites that are more readily excreted, or in some cases, may even be activated to more biologically active metabolites.[55]

Notably, Yifan Yuan et al[56] discovered that liver damage induced by Mn3O4 nanoparticles significantly upregulated the expression of CYP1A2, with the toxicity of Mn3O4 nanoparticles attributed to cytochrome P450-dependent ROS accumulation and subsequent oxidative stress. Furthermore, Ruiyue Hang et al[57] observed that micro/nanostructured molecules downregulated CYP1A2 expression, reducing mitochondrial ROS production and thereby suppressing oxidative stress and mitigating inflammation.

Furthermore, as illustrated in the study,[58] variations in CYP1A2 genetic polymorphisms can influence metabolic responses to substances such as caffeine, which may be relevant in tailoring individualized treatments in clinical settings.
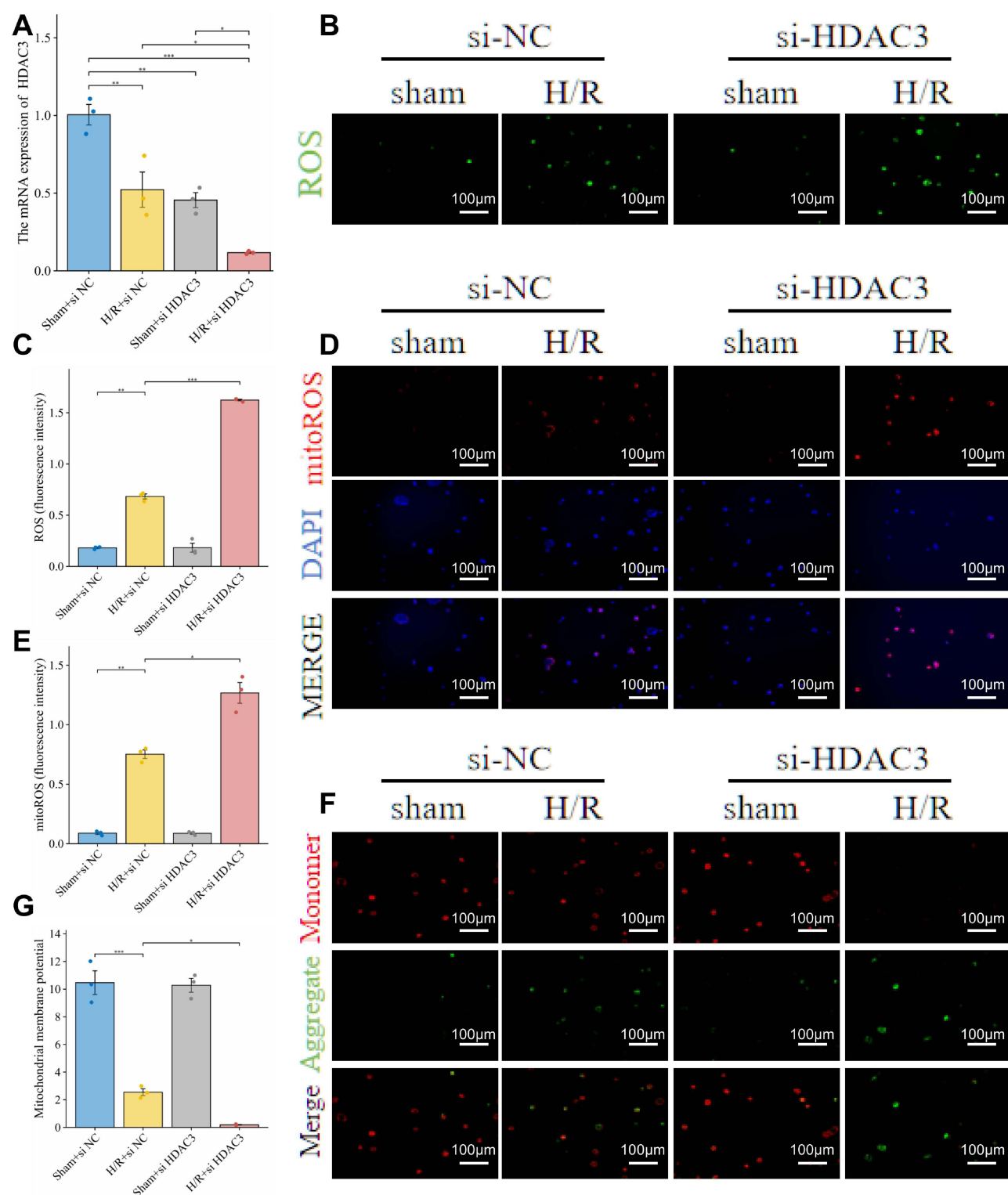
Figure 10 Knocking down HDAC3 exacerbates the oxidative stress state and mitochondrial membrane potential loss of CaCO2 cells treated with H/R. (**A**) mRNA expression level of HDAC3. (**B** and **C**) Detection of ROS levels in each group, scale bar=100 μ m. (**D** and **E**) Detection of mitoROS levels in each group, scale=100 μ m. (**F** and **G**) Detection of mitochondrial membrane potential in each group, scale=100 μ m. *: P<0.05, **: P<0.01, ***: P<0.001.
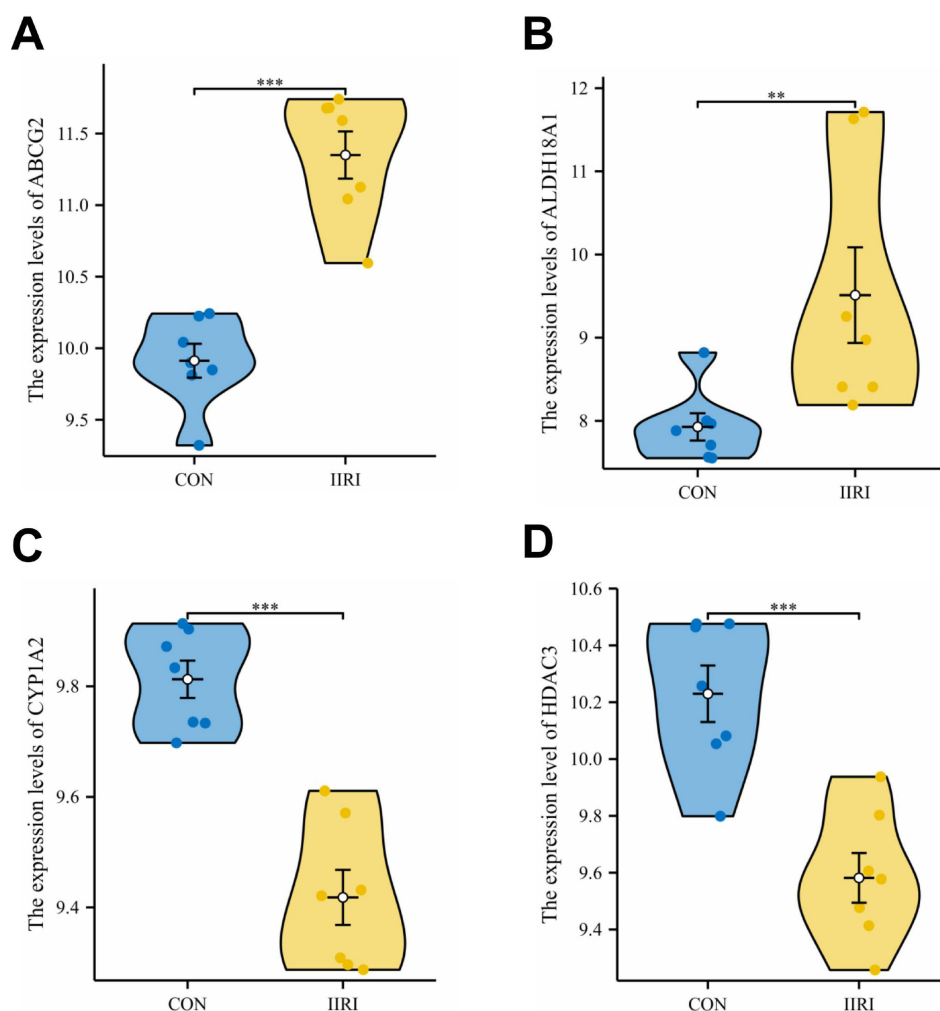
Figure 11 Prediction of Long-term Trends in IIRI HIOSRGs. (**A-D**) Expression levels of ABCG2, ALDH18A1, CYP1A2, and HDAC3 at 120 minutes of IIRI. **: P<0.01, ***: P<0.001.

Understanding how CYP1A2 affects drug metabolism and oxidative stress responses opens new avenues for optimizing therapeutic strategies for IIRI and other conditions where oxidative stress plays a pivotal role. Future research should aim to clarify the mechanisms behind CYP1A2 regulation and its implications for clinical interventions.

Our findings indicate that decreased CYP1A2 expression in IIRI may reduce oxidative stress but also suggest diminished detoxification capacity, potentially exacerbating inflammation and tissue damage.

This highlights the therapeutic potential of targeting CYP1A2 in IIRI management. Strategies to upregulate its expression or enhance activity could improve detoxification and metabolic resilience. Additionally, understanding genetic variability in CYP1A2 may allow for personalized treatment approaches, optimizing outcomes in IIRI patients. Further research is needed to clarify these mechanisms and validate therapeutic strategies.

HDAC3, a member of the histone deacetylase family, is a critical epigenetic modifier responsible for the removal of acetyl groups from histones, thereby regulating gene expression.[59,60]

As an important factor involved in gene expression regulation, HDAC3 has garnered significant attention regarding its role in oxidative stress mechanisms. The impact of HDAC3 on oxidative stress levels in various organs and diseases remains a subject of controversy. Some studies have demonstrated that the decrease in butyrate-producing bacteria and insufficient butyrate secretion contribute to increased HDAC3 activity, consequently mediating ROS production in colon disorders induced by diabetes.[61] Conversely, Xi Chen et al found that butyrate can function as an inhibitor of histone deacetylase 3, promoting ROS production through monocarboxylate transporters.[62]

Moreover, HDAC3 has a close association with mitochondrial function. HDAC3 deficiency leads to impaired mitochondrial metabolism, including alterations in the tricarboxylic acid cycle, ATP synthesis, and fatty acid metabolism, rendering mice more susceptible to high-fat diets and prone to cardiomyopathy.[63] Importantly, HDAC3 can enhance the binding between PINK1 and p53, resulting in reduced p53 acetylation, enhanced mitochondrial phagocytosis, and inhibition of inflammatory cell apoptosis.[64] Further research suggests that HDAC3 deficiency may lead to mitochondrial dysfunction, potentially linked to impaired PPAR gamma signaling.[65]

However, the relationship between HDAC3, mitochondrial functional status, and oxidative stress levels in IIRI remains unclear. In our study, we explored this relationship by transfecting siRNA-HDAC3 into CaCO2 cells. The results demonstrated that inhibiting HDAC3 expression increased ROS levels induced by IIRI while decreasing mitochondrial membrane potential, indicating that the HDAC3 oxidative stress gene plays a vital regulatory role in oxidative stress and mitochondrial ROS regulation.

Recent research has highlighted HDAC3 as a pivotal player in tumor development and therapeutic resistance, particularly in Kras-mutant non-small cell lung cancer (NSCLC). For instance, a study utilizing genetically engineered mouse models (GEMMs) demonstrated that HDAC3 is essential for lung tumor growth,[66] where it enhances the transcriptional activity of NKX2-1, a lineage-specific transcription factor. This interaction facilitates the expression of a set of common target genes, including the previously unidentified FGFR1, which plays a significant role in tumor progression. Notably, as Kras/LKB1-mutant cells develop resistance to the MEK inhibitor trametinib, an HDAC3-dependent transcriptional cassette becomes hyperactivated. This highlights the potential of HDAC3 as a target for combination therapies, as the application of the HDAC inhibitor entinostat can reverse this resistance and enhance the efficacy of trametinib.

In practical terms, this could lead to the development of combination therapies that incorporate HDAC inhibitors alongside existing treatments, such as MEK inhibitors in Kras-mutant NSCLC. By targeting HDAC3, these strategies could potentially enhance therapeutic efficacy and overcome resistance, ultimately improving patient outcomes.

Furthermore, our miRNA-mRNA network analysis revealed the intricate regulatory relationship between HIOSRGs and miRNAs, providing a fresh perspective on understanding the regulatory mechanisms of oxidative stress genes. Through in-depth exploration of the expression changes of HIOSRGs during IIRI, their connection with immune cell infiltration, and validation through animal models, we can acquire a more comprehensive understanding of the mechanisms behind oxidative stress genes in intestinal reperfusion injury.

Future research should explore the potential of targeting HIOSRGs using pharmacological agents or gene-editing techniques to delineate their therapeutic potential. Preclinical studies employing relevant animal models could assess the efficacy of these approaches in mitigating IIRI outcomes.

Lastly, translating these findings into clinical trials will be crucial. Trials designed to evaluate biomarkers associated with HIOSRGs expression and oxidative stress levels may help identify patient populations that would benefit most from targeted interventions. This multi-faceted approach will enhance our understanding of IIRI and could lead to innovative treatment strategies aimed at improving patient prognosis.

This study elucidates the interplay between oxidative stress genes and IIRI, offering novel insights into the potential pathogenesis and therapeutic avenues for IIRI. However, certain limitations must be acknowledged, particularly concerning the translational applicability of our findings.

Firstly, a significant portion of our data was derived from mouse models, which may not fully recapitulate the complex pathophysiological environment present in human IIRI. Interspecies differences in genetics, immune responses, and tissue architecture can influence the relevance of the observed oxidative stress-related mechanisms and the efficacy of potential therapeutic interventions identified in this study. Thus, while our findings provide foundational insights, the translation of these results into human therapies necessitates further validation in clinical settings, including trials that involve human tissues or relevant humanized models.

Conclusion

In conclusion, this study integrates bioinformatics and experiment validation to elucidate the significance of HIOSRGs in the progression of IIRI and explores their correlation with oxidative stress. The alterations in expression of the four HIOSRGs in IIRI may signify the cellular regulatory response to oxidative stress, warranting further investigation into

their mechanisms of action. These findings offer valuable insights for a more profound comprehension of the pathological mechanisms underlying IIRI, the exploration of novel treatment strategies, and the generation of fresh perspectives for future disease research and clinical interventions.

Abbreviations

IIRI, Intestinal ischemia-reperfusion injury; GEO, Gene Expression Omnibus; IOSRGs, IIRI oxidative stress related genes; HIOSRGs, hub IOSRGs; PCA, principal component analysis; ROC, Receiver Operating Characteristic; H/R, hypoxia/reoxygenation; DEGs, differentially expressed genes; SPF, specific pathogen-free; PPI, protein-protein interaction; P5CS, δ-1-pyrroline-5-carboxylate synthase; P5C, δ-1-pyrroline-5-carboxylate; ROS, reactive oxygen species; COPD, chronic obstructive pulmonary disease; ccRCC, clear cell renal cell carcinoma; ABC, ATP Binding Cassette; CYP, cytochrome P450.

Data Sharing Statement

All relevant data obtained or examined during the course of this study have been thoroughly incorporated into the main body of this article. The gene expression data GSE37013 was obtained from the GEO database, and the datasets analyzed in the present study are available in the GEO repository [https://www.ncbi.nlm.nih.gov/geo].

Ethics Approval and Consent to Participate

The animal experiments were approved by the Second Affiliated Hospital of Guangxi Medical University Ethical Review Committee (2024-KY(0756)). The experimental procedures followed the ARRIVE guidelines (https://arrivalguidelines.org). The animal experiments followed the Guiding Opinions on the Humane Treatment of Laboratory Animals issued by the Ministry of Science and Technology of the People's Republic of China, and the National Standard GB/T35892-2018, which is titled Ethical Standards for Animal Welfare in Experimental Research.

This study involves research on Caco-2 cells and human databases. We strictly adhere to the relevant legal regulations and have obtained ethical approval from the Ethical Review Committee of the Second Affiliated Hospital of Guangxi Medical University (2024-KY(0816)).

Funding

Disclosure

The authors report no conflicts of interest in this work.

References

1. Yu H, Kirkpatrick IDC. An update on acute mesenteric ischemia. *Can Assoc Radiol J*. 2023;74(1):160–171. doi:10.1177/08465371221094280

2. Gonzalez LM, Moeser AJ, Blikslager AT. Animal models of ischemia-reperfusion-induced intestinal injury: progress and promise for translational research. *Am J Physiol Gastrointest Liver Physiol*. 2015;308(2):G63–75. doi:10.1152/ajpgi.00112.2013

3. Niu Q, Du F, Yang X, Yang X, Wang X. Carbon monoxide-releasing molecule 2 inhibits inflammation associated with intestinal ischemia-reperfusion injury in a rat model of hemorrhagic shock. *Int Immunopharmacol*. 2022;113(Pt B):109441. doi:10.1016/j.intimp.2022.109441

4. Wang Z, Sun R, Wang G, et al. SIRT3-mediated deacetylation of PRDX3 alleviates mitochondrial oxidative damage and apoptosis induced by intestinal ischemia/reperfusion injury. *Redox Biol*. 2020;28:101343. doi:10.1016/j.redox.2019.101343

5. Schellekens D, Reisinger KW, Lenaerts K, et al. SM22 a plasma biomarker for human transmural intestinal ischemia. *Ann Surg*. 2018;268(1):120–126. doi:10.1097/SLA.0000000000002278

6. Gu L, Wang F, Wang Y, et al. Naringin protects against inflammation and apoptosis induced by intestinal ischemia-reperfusion injury through deactivation of cGAS-STING signaling pathway. *Phytother Res*. 2023;37(8):3495–3507. doi:10.1002/ptr.7824

7. Wong YL, Lautenschläger I, Hummitzsch L, et al. Effects of different ischemic preconditioning strategies on physiological and cellular mechanisms of intestinal ischemia/reperfusion injury: implication from an isolated perfused rat small intestine model. *PLoS One*. 2021;16(9):e0256957. doi:10.1371/journal.pone.0256957

8. Wan Z, Zhang Y, Lv J, Yuan Y, Guo W, Leng Y. Exosomes derived from bone marrow mesenchymal stem cells regulate pyroptosis via the miR-143-3p/myeloid differentiation factor 88 axis to ameliorate intestinal ischemia-reperfusion injury. *Bioengineered*. 2023;14(1):2253414. doi:10.1080/21655979.2023.2253414

9. Zhang FL, Chen XW, Wang YF, et al. Microbiota-derived tryptophan metabolites indole-3-lactic acid is associated with intestinal ischemia/reperfusion injury via positive regulation of YAP and Nrf2. *J Transl Med*. 2023;21(1):264. doi:10.1186/s12967-023-04109-3

10. Shen X, Shi H, Chen X, et al. Esculetin alleviates inflammation, oxidative stress and apoptosis in intestinal ischemia/reperfusion injury via Targeting SIRT3/AMPK/mTOR signaling and regulating autophagy. *J Inflamm Res*. 2023;16:3655–3667. doi:10.2147/JIR.S413941

11. Wang X, Shen T, Lian J, et al. Resveratrol reduces ROS-induced ferroptosis by activating SIRT3 and compensating the GSH/GPX4 pathway. *Mol Med*. 2023;29(1):137. doi:10.1186/s10020-023-00730-6

12. Liu M, Wen H, Zuo L, et al. Bryostatin-1 attenuates intestinal ischemia/reperfusion-induced intestinal barrier dysfunction, inflammation, and oxidative stress via activation of Nrf2/HO-1 signaling. *FASEB j*. 2023;37(6):e22948. doi:10.1096/fj.202201540R

13. Wang F, Huang H, Wei X, Tan P, Wang Z, Hu Z. Targeting cell death pathways in intestinal ischemia-reperfusion injury: a comprehensive review. *Cell Death Discov*. 2024;10(1):112.

14. Lin D, Zhang Y, Wang S, et al. Ganoderma lucidum polysaccharide peptides GL-PPSQ(2) alleviate intestinal ischemia-reperfusion injury via inhibiting cytotoxic neutrophil extracellular traps. *Int J Biol Macromol*. 2023;244:125370. doi:10.1016/j.ijbiomac.2023.125370

15. Liao SS, Zhang LL, Zhang YG, et al. Ghrelin alleviates intestinal ischemia-reperfusion injury by activating the GHSR-1α/Sirt1/FOXO1 pathway. *FASEB j*. 2024;38(11):e23681. doi:10.1096/fj.202302155RRR

16. Fan Q, Chang H, Tian L, Zheng B, Liu R, Li Z. Methane saline suppresses ferroptosis via the Nrf2/HO-1 signaling pathway to ameliorate intestinal ischemia-reperfusion injury. *Redox Rep*. 2024;29(1):2373657. doi:10.1080/13510002.2024.2373657

17. Li A, Zhang K, Zhou J, et al. Bioinformatics and experimental approach identify lipocalin 2 as a diagnostic and prognostic indicator for lung adenocarcinoma. *Int J Biol Macromol*. 2024;272(Pt 2):132797.

18. Li K, Zhang C, Zhou R, et al. Single cell analysis unveils B cell-dominated immune subtypes in HNSCC for enhanced prognostic and therapeutic stratification. *Int J Oral Sci*. 2024;16(1):29. doi:10.1038/s41368-024-00292-1

19. Wang S, Wang R, Hu D, Zhang C, Cao P, Huang J. Machine learning reveals diverse cell death patterns in lung adenocarcinoma prognosis and therapy. *NPJ Precis Oncol*. 2024;8(1):49. doi:10.1038/s41698-024-00538-5

20. Zhou H, Jing S, Liu Y, et al. Identifying the key genes of Epstein-Barr virus-regulated tumour immune microenvironment of gastric carcinomas. *Cell Prolif*. 2023;56(3):e13373. doi:10.1111/cpr.13373

21. Chi Z, Chen S, Xu T, et al. Histone deacetylase 3 couples mitochondria to drive il-1β-dependent inflammation by configuring fatty acid oxidation. *Mol Cell*. 2020;80(1):43–58.e47. doi:10.1016/j.molcel.2020.08.015

22. Li N, Liu B, Xiong R, Li G, Wang B, Geng Q. HDAC3 deficiency protects against acute lung injury by maintaining epithelial barrier integrity through preserving mitochondrial quality control. *Redox Biol*. 2023;63:102746. doi:10.1016/j.redox.2023.102746

23. Li Y, Yu J, Li R, Zhou H, Chang X. New insights into the role of mitochondrial metabolic dysregulation and immune infiltration in septic cardiomyopathy by integrated bioinformatics analysis and experimental validation. *Cell Mol Biol Lett*. 2024;29(1):21. doi:10.1186/s11658-024-00536-2

24. Shang Y, Wang X, Su S, et al. Identifying of immune-associated genes for assessing the obesity-associated risk to the offspring in maternal obesity: a bioinformatics and machine learning. *CNS Neurosci Ther*. 2024;30(3):e14700. doi:10.1111/cns.14700

25. Liu F, Huang Y, Liu F, Wang H. Identification of immune-related genes in diagnosing atherosclerosis with rheumatoid arthritis through bioinformatics analysis and machine learning. *Front Immunol*. 2023;14:1126647. doi:10.3389/fimmu.2023.1126647

26. Jiang H, Hu Y, Zhang Z, Chen X, Gao J. Identification of metabolic biomarkers associated with nonalcoholic fatty liver disease. *Lipids Health Dis*. 2023;22(1):150. doi:10.1186/s12944-023-01911-2

27. Deng B, Liao F, Liu Y, et al. Comprehensive analysis of endoplasmic reticulum stress-associated genes signature of ulcerative colitis. *Front Immunol*. 2023;14:1158648. doi:10.3389/fimmu.2023.1158648

28. Weng J, Wu XF, Shao P, Liu XP, Wang CX. Medicine for chronic atrophic gastritis: a systematic review, meta- and network pharmacology analysis. *Ann Med*. 2023;55(2):2299352. doi:10.1080/07853890.2023.2299352

29. Fan J, Shi S, Qiu Y, Liu M, Shu Q. Analysis of signature genes and association with immune cells infiltration in pediatric septic shock. *Front Immunol*. 2022;13:1056750. doi:10.3389/fimmu.2022.1056750

30. Xiao Y, Yuan Y, Yang Y, et al. GCH1 reduces LPS-induced alveolar macrophage polarization and inflammation by inhibition of ferroptosis. *Inflamm Res*. 2023;72(10–11):1941–1955. doi:10.1007/s00011-023-01785-1

31. Zhang Z, Zhu H, Wang X, Lin S, Ruan C, Wang Q. A novel basement membrane-related gene signature for prognosis of lung adenocarcinomas. *Comput Biol Med*. 2023;154:106597. doi:10.1016/j.compbiomed.2023.106597

32. Sultana A, Alam MS, Liu X, et al. Single-cell RNA-seq analysis to identify potential biomarkers for diagnosis, and prognosis of non-small cell lung cancer by using comprehensive bioinformatics approaches. *Transl Oncol*. 2023;27:101571. doi:10.1016/j.tranon.2022.101571

33. Zhao P, Zhen H, Zhao H, Huang Y, Cao B. Identification of hub genes and potential molecular mechanisms related to radiotherapy sensitivity in rectal cancer based on multiple datasets. *J Transl Med*. 2023;21(1):176. doi:10.1186/s12967-023-04029-2

34. An W, Zhou J, Qiu Z, et al. Identification of crosstalk genes and immune characteristics between Alzheimer's disease and atherosclerosis. *Front Immunol*. 2024;15:1443464. doi:10.3389/fimmu.2024.1443464

35. Marco-Marín C, Escamilla-Honrubia JM, Llácer JL, Seri M, Panza E, Rubio V. Δ(1) -Pyrroline-5-carboxylate synthetase deficiency: an emergent multifaceted urea cycle-related disorder. *J Inherit Metab Dis*. 2020;43(4):657–670. doi:10.1002/jimd.12220

36. Chen YJ, Zhang ZQ, Wang MW, et al. Novel compound missense and intronic splicing mutation in ALDH18A1 causes autosomal recessive spastic paraplegia. *Front Neurol*. 2021;12:627531. doi:10.3389/fneur.2021.627531

37. Leung KT, Chan KY, Ma TP, et al. Dysregulated expression of arginine metabolic enzymes in human intestinal tissues of necrotizing enterocolitis and response of CaCO2 cells to bacterial components. *J Nutr Biochem*. 2016;29:64–72. doi:10.1016/j.jnutbio.2015.10.010

38. Kay EJ, Zanivan S, Rufini A. Proline metabolism shapes the tumor microenvironment: from collagen deposition to immune evasion. *Curr Opin Biotechnol*. 2023;84:103011. doi:10.1016/j.copbio.2023.103011

39. Sena F, Monza J, Signorelli S. Determination of Free Proline in Plants. *Methods mol Biol*. 2024;2798:183–194.

40. Ma C, Liao K, Wang J, Li T, Liu L. L-Arginine, as an essential amino acid, is a potential substitute for treating COPD via regulation of ROS/ NLRP3/NF-κB signaling pathway. *Cell Biosci*. 2023;13(1):152. doi:10.1186/s13578-023-00994-9

41. Margolis A, Liu L, Porwollik S, et al. Arginine metabolism powers salmonella resistance to oxidative stress. *Infect Immun*. 2023;91(6):e0012023. doi:10.1128/iai.00120-23

42. Wei Q, Dong HL, Pan LY, et al. Clinical features and genetic spectrum in Chinese patients with recessive hereditary spastic paraplegia. *Transl Neurodegener*. 2019;8(1):19. doi:10.1186/s40035-019-0157-9

43. Wu G, Li T, Chen Y, et al. Deciphering glutamine metabolism patterns for malignancy and tumor microenvironment in clear cell renal cell carcinoma. *Clin Exp Med*. 2024;24(1):152. doi:10.1007/s10238-024-01390-4

44. Gunes Y, Blanco-Paniagua E, Anlas C, et al. Role of the Abcg2 transporter in plasma, milk, and tissue levels of the anthelmintic monepantel in mice. *Chem Biol Interact*. 2024;398:111117. doi:10.1016/j.cbi.2024.111117

45. Ben Halima N, Álvarez-Fernández L, Blanco-Paniagua E, Abid-Essefi S, Guedri Y, Merino G. In vitro interaction of the pesticides flupyradifurone, bupirimate and its metabolite ethirimol with the ATP-binding cassette transporter G2 (ABCG2). *Toxicol Lett*. 2023;380:23–30. doi:10.1016/j. toxlet.2023.03.012

46. Gil-Martins E, Barbosa DJ, Silva V, Remião F, Silva R. Dysfunction of ABC transporters at the blood-brain barrier: role in neurological disorders. *Pharmacol Ther*. 2020;213:107554. doi:10.1016/j.pharmthera.2020.107554

47. Tian S, Yong M, Zhu J, et al. Enhancement of the effect of methyl pyropheophorbide-a-mediated photodynamic therapy was achieved by increasing ROS through inhibition of Nrf2-HO-1 or Nrf2-ABCG2 signaling. *Anticancer Agents Med Chem*. 2017;17(13):1824–1836. doi:10.2174/ 1871520617666170327145857

48. Nie S, Huang Y, Shi M, et al. Protective role of ABCG2 against oxidative stress in colorectal cancer and its potential underlying mechanism. *Oncol Rep*. 2018;40(4):2137–2146. doi:10.3892/or.2018.6594

49. Jiang X, Chen C, Gu S, Zhang Z. Regulation of ABCG2 by nuclear factor kappa B affects the sensitivity of human lung adenocarcinoma A549 cells to arsenic trioxide. *Environ Toxicol Pharmacol*. 2018;57:141–150. doi:10.1016/j.etap.2017.12.011

50. Bauer M, Karch R, Wulkersdorfer B, et al. A proof-of-concept study to inhibit ABCG2- and ABCB1-mediated efflux transport at the human blood-brain barrier. *J Nucl Med*. 2019;60(4):486–491. doi:10.2967/jnumed.118.216432

51. Guo J, Zhu X, Badawy S, et al. Metabolism and mechanism of human cytochrome P450 enzyme 1A2. *Curr Drug Metab*. 2021;22(1):40–49. doi:10.2174/18755453MTEyCOTgcx

52. Fekete F, Menus Á, Tóth K, et al. CYP1A2 expression rather than genotype is associated with olanzapine concentration in psychiatric patients. *Sci Rep*. 2023;13(1):18507. doi:10.1038/s41598-023-45752-6

53. Fathi MA, Han G, Kang R, Shen D, Shen J, Li C. Disruption of cytochrome P450 enzymes in the liver and small intestine in chicken embryos in ovo exposed to glyphosate. *Environ Sci Pollut Res Int*. 2020;27(14):16865–16875. doi:10.1007/s11356-020-08269-3

54. Gerges SH, El-Kadi AOS. Sexual dimorphism in the expression of cytochrome P450 enzymes in rat heart, liver, kidney, lung, brain, and small intestine. *Drug Metab Dispos*. 2023;51(1):81–94. doi:10.1124/dmd.122.000915

55. Spatzenegger M, Horsmans Y, Verbeeck RK. Differential activities of CYP1A isozymes in hepatic and intestinal microsomes of control and 3-methylcholanthrene-induced rats. *Pharmacol Toxicol*. 2000;86(2):71–77. doi:10.1034/j.1600-0773.2000.pto860205.x

56. Yue Z, Zhang X, Yu Q, Liu L, Zhou X. Cytochrome P450-dependent reactive oxygen species (ROS) production contributes to Mn3O4 nanoparticle-caused liver injury. *RSC Adv*. 2018;8(65):37307–37314. doi:10.1039/C8RA05633A

57. Hang R, Zhao Y, Zhang Y, et al. The role of nanopores constructed on the micropitted titanium surface in the immune responses of macrophages and the potential mechanisms. *J Mater Chem B*. 2022;10(38):7732–7743. doi:10.1039/D2TB01263D

58. Varillas-Delgado D, Coso JD, Muñoz A, Aguilar-Navarro M, Gutierrez-Hellin J. Influence of the CYP1A2 c.(−163) A > C polymorphism in the effect of caffeine on fat oxidation during exercise: a pilot randomized, double-blind, crossover, placebo-controlled trial. *Eur J Nutr*. 2024;63 (7):2697–2708. doi:10.1007/s00394-024-03454-3

59. Xiao Y, Hale S, Awasthee N, et al. HDAC3 and HDAC8 PROTAC dual degrader reveals roles of histone acetylation in gene regulation. *Cell Chem Biol*. 2023;30(11):1421–1435.e1412. doi:10.1016/j.chembiol.2023.07.010

60. Li N, Liu B, He R, et al. HDAC3 promotes macrophage pyroptosis via regulating histone deacetylation in acute lung injury. *iScience*. 2023;26 (7):107158. doi:10.1016/j.isci.2023.107158

61. Noureldein MH, Bitar S, Youssef N, Azar S, Eid AA. Butyrate modulates diabetes-linked gut dysbiosis: epigenetic and mechanistic modifications. *J Mol Endocrinol*. 2020;64(1):29–42. doi:10.1530/JME-19-0132

62. Chen X, Xie X, Sun N, et al. Gut microbiota-derived butyrate improved acute leptospirosis in hamster via promoting macrophage ROS mediated by HDAC3 inhibition. *mBio*. 2024;15(10):e0190624. doi:10.1128/mbio.01906-24

63. Sun Z, Singh N, Mullican SE, et al. Diet-induced lethality due to deletion of the Hdac3 gene in heart and skeletal muscle. *J Biol Chem*. 2011;286 (38):33301–33309. doi:10.1074/jbc.M111.277707

64. Zhang Q, Liu XM, Hu Q, et al. Dexmedetomidine inhibits mitochondria damage and apoptosis of enteric glial cells in experimental intestinal ischemia/reperfusion injury via SIRT3-dependent PINK1/HDAC3/p53 pathway. *J Transl Med*. 2021;19(1):463. doi:10.1186/s12967-021-03027-6

65. Yao Y, Liu Q, Adrianto I, et al. Histone deacetylase 3 controls lung alveolar macrophage development and homeostasis. *Nat Commun*. 2020;11 (1):3822. doi:10.1038/s41467-020-17630-6

66. Eichner LJ, Curtis SD, Brun SN, et al. HDAC3 is critical in tumor development and therapeutic resistance in Kras-mutant non-small cell lung cancer. *Sci Adv*. 2023;9(11):eadd3243. doi:10.1126/sciadv.add3243